Materials Science in Semiconductor Processing 82 (2018) 126–134

Contents lists available at ScienceDirect

Materials Science in Semiconductor Processing

journal homepage: www.elsevier.com/locate/mssp

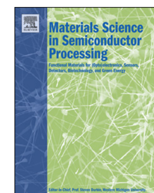

Codoping effects of the Zn acceptor on the structural characteristics and electrical properties of the Ge donor-doped GaN thin films and its hetero-junction diodes all made by reactive sputtering

Cao Phuong Thao[a], Dong-Hau Kuo[a,*], Der-Jun Jan[b]

[a] Department of Materials Science and Engineering, National Taiwan University of Science and Technology, Taipei 10607, Taiwan
[b] Physics Division, Institute of Nuclear Energy Research (INER), Longtan District, Taoyuan City 32546, Taiwan

ARTICLE INFO

Keywords:
Zn acceptor
Ge donor
GaN
Sputtering
Thin film
Electrical property

ABSTRACT

Zn acceptor/Ge donor (Zn/Ge)-codoped GaN films with different Zn contents have been deposited on Si substrates at 300 °C and at 90–150 W by RF reactive sputtering technique with cermet targets at the composition atomic ratios of Zn:Ge:(Ga + GaN) at x:0.03:(0.97-x) with x = 0, 0.03, 0.06, and 0.09 and Ga:GaN = 3:7. The films made with such targets were presented in an abbreviated symbol of Zn-x-GeGaN at x = 0, 0.03, 0.06, and 0.09. The morphology, structure, electrical properties, optical property, and hetero-junction diode devices involved in the Zn-x-GeGaN films were thoroughly investigated. The systematic Zn increment into the n-type Zn-0-GeGaN through property evaluation provides the supporting information in studying solid solutioning. Zn-x-GeGaN films converted into p-type semiconductor at x = 0.06 and 0.09. The values of bandgap were in the range of 2.87–3.17 eV with the lower value for the higher Zn content in Zn-x-GeGaN films. The higher RF power led to the faster growth, highly deficient in nitrogen, and a higher Zn atom ratio in the deposited film. The 120W-deposited Zn-0.06-GeGaN film had hole concentration of 7.21×10^{16} cm^{-3}, hole mobility of 39.1 cm^2 V^{-1} s^{-1}, and the electrical conductivity of 0.45 S/cm.

1. Introduction

GaN semiconductor material has the wide direct bandgap and interesting characteristics such as high breakdown voltage, high mobility, and thermal stability [1]. It has been realized that GaN and its alloys are employed in blue-light-emitting diodes (LEDs) and laser diodes (LDs) [2,3]. In 2014, Prof. S. Nakamura won the Nobel Prize for Physics and he showed that defect technology to control the electrical properties of GaN, which has been promising for the evolution of the p-type Mg-doped GaN in realizable the commercialization GaN-based LEDs. Alloy systems in GaN, Mg-GaN and In-GaN had been studied and the n-type doped properties were modified by efforts in Si-, Ge-, and Sn-doped GaN [4,5], while codoping GaN with Si donor and Zn acceptor was also reported [6,7]. Additionally, p-type GaN with high hole concentration becomes a key material for the improvement in photo-electronic and electronic devices [8–11]. However, fabrication of p-type doping is known to be hard for semiconductor with low valence-band maximum (VBM) energy, while it is difficult to obtain the high conduction-band minimum (CBM) energy in n-type doping by compensation and bipolar doping [12,13]. To overcome the drawback of p-type and n-type doping, the codoping technique has been used to effectively tune the dopant concentrations and properties of electronic and magnetic devices [14]. The codoping method can effectively increase the solubility of dopant and the rate of activation by an increment of the electrical mobility and the reduction of carrier ionization energy [15]. Katayama et al. [16] proposed the concept of codoping in which the donor and acceptor were doped at the same time to prepare p-type GaN with low resistivity. They doped Mg and Si into the lattice of GaN at a concentration of 2: 1. As a result, the acceptor energy level was decreased by codoping and the film was enhanced in the solid solubility of the dopant, electrical mobility, and carrier concentration. Besides, Kim et al. studied the doping Mg and Si in GaN by metalorganic chemical vapor deposition (MOCVD) in 1999. It was explained that the concept of competitive adsorption between Mg and Si during the deposition process to get the characteristics of Mg-Si codoping and to make p-GaN high electrical conductivity [17]. In 2000, Kim et al. [18] investigated the characteristics of Zn-Mg codoped GaN film deposited by metalorganic chemical vapor deposition technology. S. Nakamura et al. [19] mentioned that codoped Si and Zn in InGaN formed donor and deep acceptor energy levels, respectively. Sheu's research team [20] codoped Si and Zn atoms in InGaN by metal-organic vapor-phase epitaxy (MOVPE) in 2002 to form the donor and deep acceptor energy levels. In

* Corresponding author.
E-mail addresses: d10404808@mail.ntust.edu.tw (C.P. Thao), dhkuo@mail.ntust.edu.tw (D.-H. Kuo).

https://doi.org/10.1016/j.mssp.2018.04.002
Received 9 January 2018; Received in revised form 31 March 2018; Accepted 2 April 2018
1369-8001/ © 2018 Published by Elsevier Ltd.

2012, M. A. Reshchikov et al. [7] measured the internal quantum efficiency (IQE) of codoped Si/Zn GaN films as high as 90% by using time-resolved photoluminescence (TRPL). They used the MOVPE method to grow n-type GaN: Si, Zn thin films on a sapphire substrate with a carrier concentration of (0.75–1.14) $\times 10^{19}$ cm^{-3} and carrier mobility of 150 cm^2 V^{-1} s^{-1} at room temperature.

In recent years, our group has successfully employed the RF reactive sputtering technique for the III-nitride compounds with single cermet targets to replace the pure Ga visco-liquid target [21–25]. The RF reactive sputtering technology provides an easy-accessible, easy-to-clean, and low-cost method and the targets used for this method have been designed in a wide range of the composition. Consequently, the study of acceptor/donor doping in semiconductors of III-nitride compound especially GaN can be easily executed. The sputtered *p*-type GaN and InGaN film had been achieved [21–23]. To study the effects of doping on the semiconductor properties, a systematic change in film composition is the basic strategy to study the solid solubility, the structure, properties, and their relationship for the purpose of understanding the possible defect nature.

In this work, we successfully grew Zn acceptor/Ge donor (Zn/Ge)-codoped GaN films on Si substrates by RF reactive sputtering technique with cermet targets at the metallic composition ratios of Zn:Ge:(Ga + GaN) = x:0.03:(0.97-x) with x = 0, 0.03, 0.06, and 0.09 and at Ga: GaN = 3:7. The targets were represented with the abbreviated symbol of Zn-x-GeGaN at x = 0, 0.03, 0.06, and 0.09, while its formed films were named as Zn-x-GeGaN films. The variation of the Zn content in Zn-x-GeGaN films can provide clear evidences for the study of the effect of point defects on film properties. The hetero-junction p-n diodes made with Zn-x-GeGaN films and *p*- or *n*-type Si substrates were also fabricated to evaluate the diode performance.

2. Experimental details

Zn/Ge-codoped GaN thin films were grown on Si substrates by RF reactive sputtering technology with a cermet target in the Ar and N_2 mixed atmosphere. The targets were made by hot pressing with the mixture of metallic Zn, Ga and Ge powders and ceramic GaN powder. After the cermet targets were fabricated by hot pressing at 300 °C for 1 h under argon, the corresponding films made with Zn-x-GeGaN targets were indicated as Zn-x-GeGaN films at x = 0, 0.03, 0.06 and 0.09. To avoid the oxygen and impurities, mechanical and diffusion pumps were employed to pump the chamber pressure down to 1×10^{-6} Torr before sputtering. To get rid of surface contamination of target from hot pressing, the first run with each target was the test run and used to clean the target surface with plasma for 1 h. During the formal depositing process, the substrate temperature was set at 300 °C and the gas admixture of Ar and N_2 flow was kept at a flow rate of 5 sccm and 15 sccm, respectively. The working pressure was fixed at 9×10^{-3} Torr while the RF sputtering power was 120 W and deposition time 30 min. The single cermet targets used in RF sputtering were 5.08 cm (2 in.) in the size and the working distance between target and substrates in chamber for sputtering was fixed at 5 cm. To study the influences of output RF power for sputtering on Zn-x-GeGaN films, the Zn-0.06-GeGaN target was used to to deposit films at sputtering power of 90–150 W. The choice of Zn-0.06-GeGaN target for films at different powers was based upon the performance data from the different Zn-x-GeGaN films at x = 0, 0.03, 0.06, and 0.09, with which the n-type → p-type conversion is expected to occur for the valuable p-type Zn-x-GeGaN.

The hetero-junction diode was also made by RF sputtering technique. The Zn-x-GeGaN films were deposited on the *n*-Si (100) or *p*-Si (100) substrates. The diodes owned the ohmic contact, as Al with low work function was selected for contact with the n-type layer (n-Si substrate or n-GaN based film) and Pt with the high work function was selected for contact with the p-type layer (p-Si substrate or p-GaN based film). The hetero-junction devices named device-A and device-B were made by the Zn-0-GeGaN and Zn-0.03-GeGaN films deposited on *p*-Si substrates, respectively. The *p*-Zn-GeGaN/*n*-Si hetero-junction diodes were fabricated by the Zn-0.06-GeGaN and Zn-0.09-GeGaN films grown on *n*-Si substrates to form device-C and device-D, respectively. Those above-mentioned diodes were deposited on Si wafer with the "top-top" electrode designing. The n-Si (100) wafer with polished surface had sheet resistance of ~ 1–10 Ω cm, thickness of ~ 550 µm, the carrier concentration of ~10^{15} cm^{-3}, and mobility of ~ 200 cm^2/V s. Besides, the boron-doped p-Si(100) wafer had a flat surface, the sheet resistance of ~ 1–10 Ω cm, the thickness of ~ 650 µm. Pt and Al metals were, respectively, used to make Ohmic contacts with the *p*- and *n*-type semiconductors for diodes. The electrodes were deposited at 200 °C for 30 min with the pure Al and Pt targets (99.999%) on the tops of film. The detailed processes for making the diodes with our sputtered III-nitride films were mentioned in our previous work [10,21,24,26,27].

X–ray diffractometry (XRD, D8 Discover, Bruker) and high–-resolution transmission electron microscopy (HRTEM, Technai G2, Philips) were employed to study the structure of crystalline Zn-x-GeGaN films. The morphology of surface and cross-section images of the Zn-x-GeGaN films were observed by scanning electron microscopy (SEM, JSM-6500F, JEOL). Atomic force microscopy (AFM, Dimension Icon, Bruker) was used to determine the topography of surface and the root-mean-square (*rms*) values of roughness of these films. The compositional analyses of Zn-x-GeGaN films were proceeded by the energy dispersive spectrometer (EDS, JSM-6500F, JEOL) on SEM. Hall measurement system (HMS-2000, Ecopia) with a maximum magnetic field of 0.51 T was applied to measure the electrical concentration, electrical conductivity and mobility of Zn-x-GeGaN films, while their absorption spectra were tested by ultraviolet-visible (UV–Vis) spectrometer (V-670, Jasco) The electrical properties of the diodes were investigated by the I-V tests with a Semiconductor Device Analyzer (Agilent, B1500A) at room temperature.

3. Results and discussions

3.1. Influences of Zn dopant content on structural and properties of the sputtered Zn-x-GeGaN films

Table 1 shows the EDS composition analyses of Zn-x-GeGaN films with different Zn contents (x = 0, 0.03, 0.06 and 0.09) grown at 120 W in power and the temperature of 300 °C under Ar and N_2 flow of gases. The [N]/([Zn] + [Ga] + [Ge]) atomic ratios were 0.938, 0.909, 0.876 and 0.865 for Zn-x-GeGaN films at x = 0, 0.03, 0.06, and 0.09, respectively and the nitrogen composition appeared to be lower at the higher Zn content. The [Zn]/([Zn] + [Ga] + [Ge]) atomic ratios were 0, 0.047, 0.079, and 0.129, as the Zn cationic contents in cermet targets were 0, 3, 6 and 9 at%, respectively. From EDS testing data, the Zn contents in Zn-x-GeGaN films were noticeably higher than those in the targets. It is expected that there was a higher sputtering yield for Zn than other composition like Ga and GaN. Besides, the data in Table 1 also shows that the [Ge]/([Zn] + [Ga] + [Ge]) atomic ratios were 0.042, 0.036, 0.037, and 0.041 for Zn-x-GeGaN at x = 0, 0.03, 0.06, and 0.09, respectively and Ge content in films was slightly higher the expected Ge ratios of 3 at% in the sputtered targets. The basic trend in Table 1 is that the higher Zn doping content leads to the higher Zn amount and the much nitrogen deficiency or the more nitrogen vacancies in film. As the concentration of cationic Zn becomes higher, the total cation charge becomes lower. In order to have charge balance, the N content needs to be lower at the same time.

Fig. 1a presents the XRD patterns of the Zn-x-GeGaN films (x = 0, 0.03, 0.06, and 0.09) deposited by RF sputtering at power of 120 W. From the XRD investigation, all Zn-x-GeGaN films sputtered on Si substrates had a wurtzite crystal structure. The diffraction ($10\bar{1}0$), ($10\bar{1}1$) and ($11\bar{2}0$) peaks were distinctly detected from these Zn-x-GeGaN films with the preferential ($10\bar{1}0$) growth plane without second phases being found. The diffraction intensity of ($10\bar{1}0$) peak became weaker and that

Table 1
Compositional analyses of Zn-*x*-GeGaN films sputtered at the different Zn contents in targets and at various RF sputter power range of 90–150 W.

Deposition parameters		[Zn] (at%)	[Ga] (at%)	[Ge] (at%)	[N] (at%)	[Zn] /([Zn] + [Ga] + [Ge])	[Ge] /([Zn] + [Ga] + [Ge])	[N] /([Zn] + [Ga] + [Ge])
x in Zn-*x*-GeGaN	0	–	49.45	2.16	48.39	–	0.042	0.938
	0.03	2.47	48.03	1.88	47.62	0.047	0.036	0.909
	0.06	4.22	46.91	2.00	46.87	0.079	0.037	0.876
	0.09	6.93	44.46	2.22	46.39	0.129	0.041	0.865
Sputtering power (W)	90	1.33	48.65	1.65	48.37	0.026	0.032	0.937
	120	4.22	46.91	2.00	46.87	0.079	0.037	0.876
	150	6.37	46.54	2.31	44.78	0.115	0.042	0.811

of (10$\bar{1}$1) peak stronger as Zn dopant content in deposited films increased. Table 2 lists all the observed data from X-ray diffraction analyses. It displays that lattice constants of *a* and *c* and the unit cell volume of Zn-*x*-GeGaN films decreased as Zn content in the grown films increased. While the lattice constant of *c* was 5.54 Å for Zn-0-GeGaN and 5.62 Å for Zn-0.03-GeGaN, this constant dropped to 5.45 and 5.09 Å for Zn-0.06-GeGaN and Zn-0.09-GeGaN films, respectively. Besides, *a* was 3.41 Å for Zn-0-GeGaN and 3.45 Å for Zn-0.03-GeGaN, but declined to 3.35 Å for Zn-0.06-GeGaN and 3.13 Å for Zn-0.09-GeGaN. Additionally, cell volumes of Zn-*x*-GeGaN films at $x = 0$, 0.03, 0.06 and 0.09 was 55.59, 58.20, 53.02, 43.21 at Å^3, respectively. From the value of 2θ degree shown in Table 2, the full width at half maxima (FWHM) values of the (10$\bar{1}$0) peaks exhibited a slight increase from 0.26° for Zn-0-GeGaN to 0.29° for Zn-0.03-GeGaN and a dramatic rise to 0.34° for Zn-0.06-GeGaN and to 0.38° for Zn-0.09-GeGaN. Besides, the crystallite sizes calculated by the Scherer equation with the FWHM values were 34.22, 30.31, 26.04 and 23.72 nm for the Zn-*x*-GeGaN films at $x = 0$, 0.03, 0.06, and 0.09, respectively. The FWHM value of the (10$\bar{1}$0) peak was a function of crystallite size. It is indicated that there was a reduction of Zn-*x*-GeGaN crystallite sizes from 34.2 nm to 23.7 nm as the higher Zn content in films had the higher FWHM values of the (10$\bar{1}$0) peaks in Zn-*x*-GeGaN film. The effective ionic sizes of Zn, Ge, and Ga are 74, 73, and 62 p.m., respectively [24]. The increase in the Zn content in film is expected to expand the lattice and have a larger cell volume, but actually the cell volume decreased. The explanation can be related to the increase in the nitrogen vacancy content at the higher Zn content in film, as the explanation for the N content in Table 1, to lead to the shrinkage of unit cell.

Fig. 2 shows the SEM surface and cross-sectional images and the AFM morphologies of Zn-*x*-GeGaN films after scanning on the 5 × 5 μm^2 dimension of these films grown at temperature of 300 °C and 120 W in power by RF sputtering technology. The SEM surface morphologies presented that the microstructure for the deposited Zn-*x*-GeGaN films was continuous and smooth with their average grain size in nanometer scale. Fig. 2 also represents the SEM cross-sectional images to show the good adhesiveness and the interfaces between Zn-GeGaN layers and Si substrate free of cracks or voids. The thick thickness of Zn-*x*-GeGaN films decreased from 1.2 μm to 0.96 μm as Zn dopant content in film increased from 0 to 9 at%. The growth rates of Zn-*x*-GeGaN films at $x = 0$, 0.03, 0.06 and 0.09 were 40, 40, 33 and 32 nm/min, respectively, as shown in Table 3. The data showed that the film deposition rate slightly dropped at the higher Zn content. From the thickness variation, it is found that the Zn addition slows the grain growth. The reason can be attributed to the difficulty in incorporating the Zn into the Ga lattice in GaN, as they have the charge difference. To have a higher Zn substitution, the Zn-*x*-GeGaN phase formation on substrate for chemical reactions will take longer time with a slower growth rate. From the Fig. 2e-h, it has shown that the root-mean-square (rms) roughness values of Zn-*x*-GeGaN films were 1.67, 0.80, 1.61 and 2.55 nm for Zn-*x*-GeGaN films at $x = 0$, 0.03, 0.06 to 0.0.09, respectively. The incorporation of different Zn amounts in Zn-*x*-GeGaN can make the surface smooth, but a higher Zn content in film degraded the surface smoothness. The rougher surface for Zn-*x*-GeGaN at a higher Zn content can be related to the retarded surface reactions with more Zn atoms trying to be soluble into the Ga lattice in films. The growth retardation by Zn on surface kinetic reactions is consistent with the explanation for the Zn effect on the growth rate. The grown GaN film by

Table 2
Structure properties of Zn-*x*-GeGaN films at $x = 0$, 0.03, 0.06, and 0.09 and Zn-0.06-GeGaN films sputtered at sputtering powers of 90, 120, and 150 W, obtained from X-ray diffraction analyses.

Deposition parameters		2θ of (10$\bar{1}$0) peak	*a* (Å)	*c*(Å)	*Volume* (Å^3)	FWHM of (10$\bar{1}$0) (degree)	Crystallite size (nm)
x in Zn-*x*-GeGaN	0	32.35	3.41	5.54	55.59	0.26	34.2
	0.03	32.30	3.45	5.62	58.20	0.29	30.3
	0.06	32.33	3.35	5.45	53.02	0.34	26.1
	0.09	32.40	3.13	5.09	43.21	0.38	23.7
Sputtering power (W)	90	32.25	3.2	5.21	46.22	0.38	24.2
	120	32.33	3.35	5.45	53.02	0.34	26.1
	150	32.40	3.19	5.18	45.57	0.23	39.2

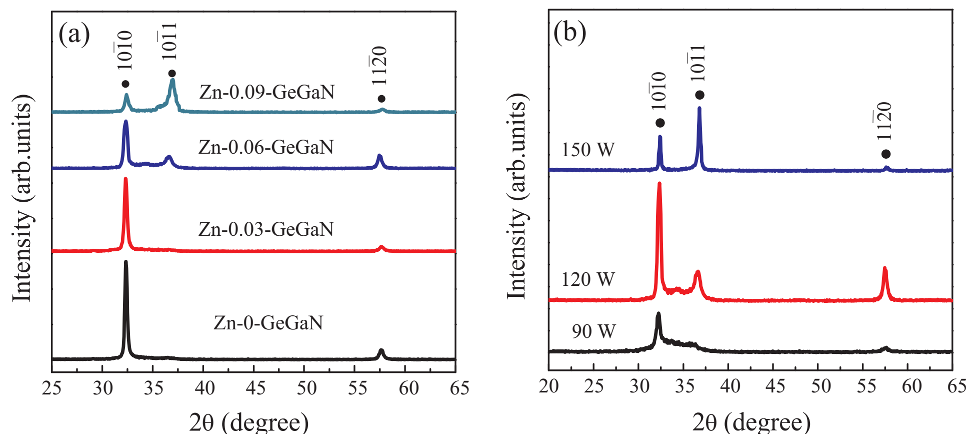

Fig. 1. XRD patterns of (a) Zn-*x*-GeGaN films at $x = 0$, 0.03, 0.06 and 0.09 and (b) Zn-0.06-GeGaN films grown at output RF powers of 90, 120, and 150 W.

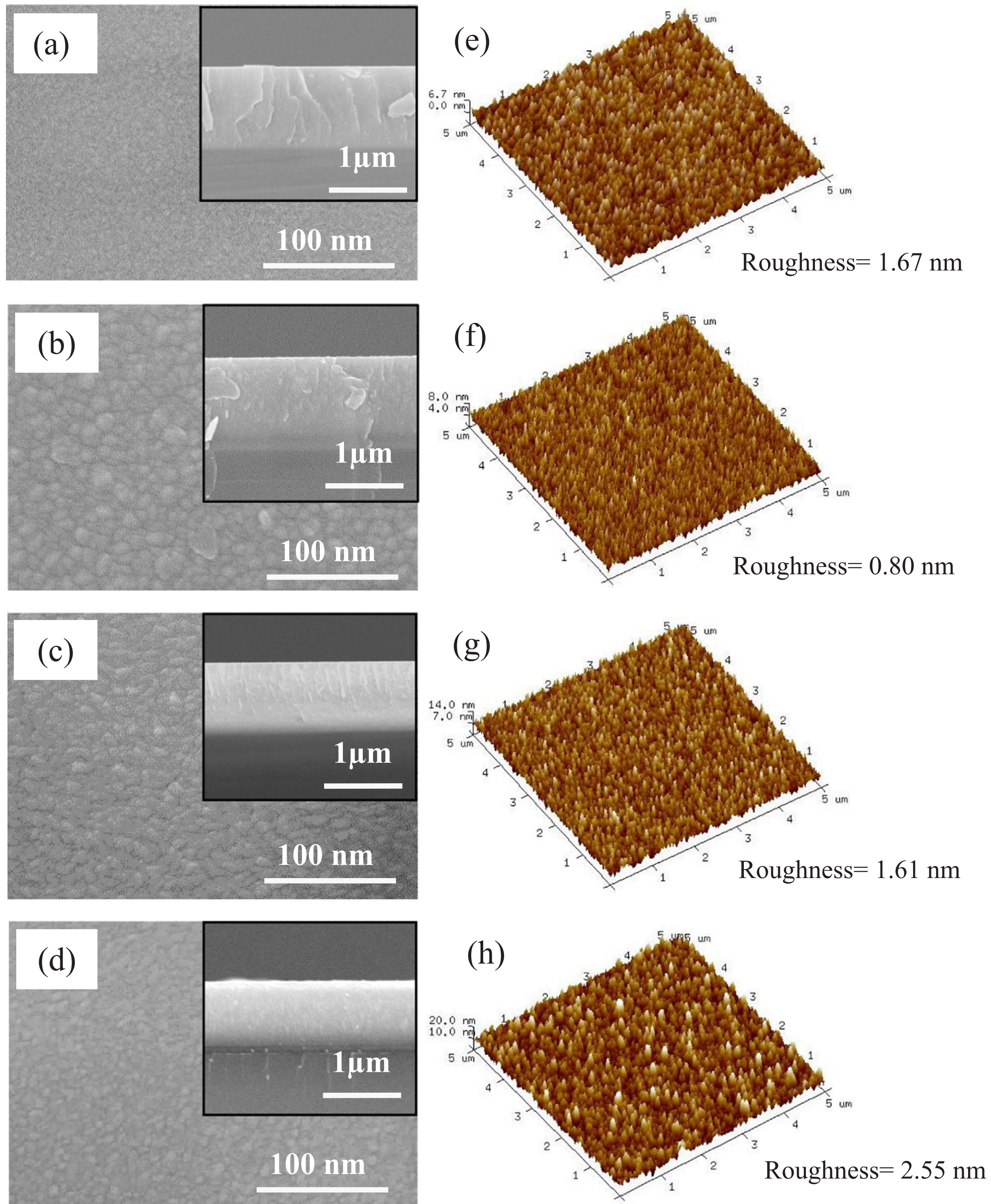

Fig. 2. (a,b,c,d) SEM surface images and (e,f,g,h) 3D AFM morphologies of Zn-x-GeGaN films at (a,e) x = 0, (b,f) x = 0.03, (c,g) x = 0.06, and (d,h) x = 0.09. The insets are their individual cross–sectional images.

RF sputtering method had the range of roughness from 0.7 to 20 nm [28], while the GaN films prepared by MOCVD system possessed roughness in the range of 0.5–3 nm [29]. Our RF reactively sputtered Zn-x-GeGaN films with the surface roughness of 0.8–2.55 nm have demonstrated its surface flatness and smoothness.

Field emission Gun Transmission Electron Microscopy (FEG-TEM) has been used to study the structure-property of the Zn-0.06-GeGaN film. As shown in Fig. 3, the high-resolution image Zn-0.06-GeGaN film indicated the (10$\bar{1}$0) plane with the calculated d-space value of 2.8 Å. There were no inclusions or second phases remained in the image. The chosen area electron diffraction (SAED) pattern of Zn-0.06-GeGaN film was presented in the inset in Fig. 3. From the SAED image, it was a ring pattern determining that structure had a characteristic of polycrystalline. The diffraction rings contributed from the (10$\bar{1}$0), (10$\bar{1}$1) and (11$\bar{2}$0) crystal planes of Zn-x-GeGaN were logically consistent with the XRD results. It is further confirmed that Zn and Ge formed the solid solution into the GaN crystal lattice.

The electrical properties of Zn-x-GeGaN films at x = 0, 0.03, 0.06, and 0.09 were tested by Hall measurement system at room temperature. Fig. 4a illustrates the electrical characteristics of Zn-x-GeGaN films (x = 0, 0.03, 0.06, and 0.09) deposited at 120 W and temperature of 300 °C for a period of 30 min. From EDS data, while Ge dopant content

Table 3
The influences of Zn content in target and RF sputtering power on the structural properties of Zn-*x*-GeGaN films.

The deposition parameters		Film thickness (nm)	Deposition rate (nm/min)	Roughness (nm)
x in Zn-*x*-GeGaN	0.0	1.20	40	1.67
	0.03	1.20	40	0.80
	0.06	1.00	33.33	1.61
	0.09	0.96	32.00	2.55
Sputtering power (W)	90	0.85	28.33	0.51
	120	1.00	33.33	1.61
	150	2.00	66.67	2.37

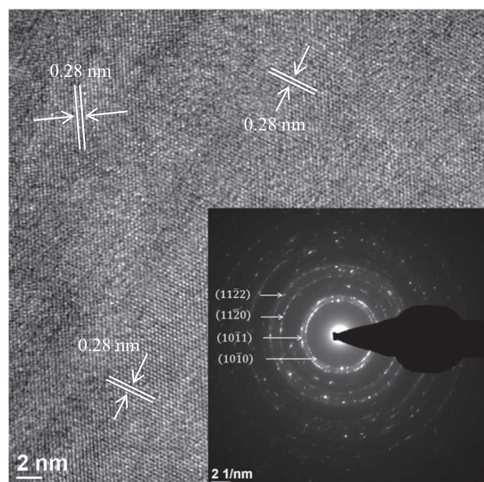

Fig. 3. FEG-TEM image of Zn-0.06-GeGaN film deposited at 300 °C and 120 W RF power in Ar/N_2 atmosphere. The inset shows the SEAD pattern of Zn-0.06-GeGaN film.

in film is close to 4 at% compared with 3 at% of Ge in sputtered target, Zn content in the deposited film was 4.7, 7.9, and 12.9 at%, as the Zn contents in cermet targets were 3, 6 and 9 at%, respectively. It is explained that the electrical properties in grown films are affected by Zn content in films. The increased Zn content in the sputtered film leads to the decrease of electron concentration in Zn-*x*-GeGaN due to the acceptor hole counteracts the donor electron. From our previous study, uncodoped-Ge-0.03-GaN film worked as *n*-type layer and contained the carrier concentration of 2.55×10^{18} cm^{-3}, electrical mobility of 3.74 cm^2 V^{-1} s^{-1}, and conductivity of 1.53 S cm^{-1} [30]. It is expected that the higher Zn dopant content of Zn-*x*-GeGaN film can provide more acceptors and more hole concentration. Thus, the electrical properties of Zn-0.03-GeGaN film maintained as *n*-type semiconductor while it had the decreased carrier concentration to 8.01×10^{15} cm^{-3} and the increased electrical mobility to 131 cm^2 V^{-1} s^{-1}. At $x = 0.06$ and 0.09, the doping amount of Zn in Zn-0.06-GeGaN and Zn-0.09-GeGaN films is 7.9, and 12.9 at%, respectively and the films were transformed from *n*-type into *p*-type semiconductor without any annealing process. The Zn-0.06-GeGaN and Zn-0.09-GeGaN films had an increment in hole concentration from 7.21×10^{16} cm^{-3} to 1.38×10^{18} cm^{-3}, respectively, while electrical mobility of these films lowered from 39.1 cm^2 V^{-1} s^{-1} to 28.6 cm^2 V^{-1} s^{-1}. The Zn content in Zn-*x*-GeGaN films increased and enhanced the hole concentration in films. Therefore, the electrons in the *n*-type could be replaced by the holes for forming the *p*-type semiconductor. It is determined that the conductivity (σ) of Zn-*x*-GeGaN films depended on electrical concentration and mobility. The σ values were 0.16 S cm^{-1} for Zn-0.03-GeGaN, 0.45 S cm^{-1} for Zn-0.06-GeGaN and 6.30 S cm^{-1} for Zn-0.09-GeGaN.

UV–Vis measurement of Zn-*x*-GeGaN films was investigated at room temperature. The Tauc equation, represented as Eq. (1), for UV–Vis database could be used to figure the coefficient of optical absorption and bandgap (E_g) of Zn-*x*-GeGaN films.

$$(\alpha hn)^2 = A\,(h\nu - E_g) \tag{1}$$

where α is optical absorption coefficient, *A* a constant, *hν* the incident photon energy, and E_g the energy bandgap of the Zn-*x*-GeGaN films. The plots of the $(\alpha h\nu)^2$-hν curves are shown in Fig. 5a and the energy bandgap of Zn-*x*-GeGaN films could be directly obtained by extrapolating the linear part of these curves. The absorption fringes in Fig. 5 can be attributed to the extremely smooth surface and the 800 nm-thick films to establish the interference fringes. As seen from the extrapolated curves, the Zn-*x*-GeGaN films at $x = 0$, 0.03, 0.06, and 0.09 had the E_g values of 3.0, 3.02, 2.98, and 2.87 eV, respectively. In this experiment, the content of Zn for Zn-*x*-GeGaN films rose from 0 at% at $x = 0$ to the highest value of 12.9% at $x = 0.09$ and their band gap slightly dropped from 3.0 to 2.87 eV, indicating the solid solutioning of Zn and Ge in GaN to form the defect levels and to lower the absorption energy. Neugebauer and his group demonstrated that the nitrogen vacancy (a donor) in *p*-type GaN contains the lowest formation energy while there was the gallium vacancy (an acceptor) in *n* type GaN [31]. Shikanai et al. proposed that ionization energy of Ge donor in GaN is 30 meV [32]. Zn formed the deeper Zn_{Ga} acceptor level located 200–400 meV above the valance band [30]. Additionally, Mattila et al. presented that acceptor energy levels for cation would be located higher the valence band, indicating a deep acceptor [33]. H. Katayama-Yoshida recommended the co-doping method with both n-type and p-type dopants co-existing at the same time [11]. In the Zn-*x*-GeGaN thin film, Ge worked as a donor and Zn an acceptor in GaN. If the GaN has Eg of 3.3 eV, the Ge donor level of 30 meV below conduction band and Zn_{Ga}

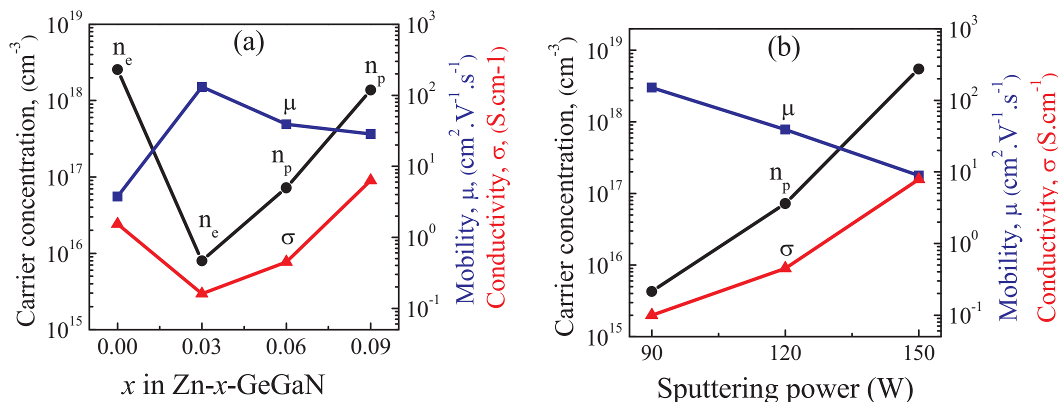

Fig. 4. (a) Electrical properties of Zn-*x*-GeGaN films at $x = 0$, 0.03, 0.06, and 0.09 and (b) electrical properties of Zn-0.06-GeGaN films deposited under different RF output powers of 90, 120, and 150 W.

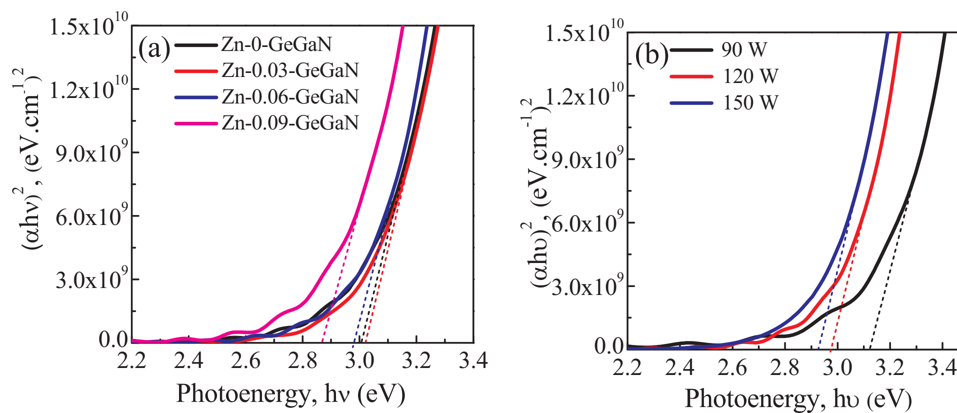

Fig. 5. Plots of $(\alpha h\nu)^2$ vs. photon energy ($h\nu$) for the optical band gap determination of (a) the Zn-*x*-GeGaN films at $x = 0$, 0.03, 0.06 and 0.09 and (b) the Zn-0.06-GeGaN films sputtered at different sputtering powers.

acceptor level of 400 meV above the valence band, the photo absorption energy is about 3.3–0.03-0.4 = 2.87 eV, equal to the E_g of Zn-0.09-GeGaN. This evidence further supports the coexistence of donor and acceptor in Zn-*x*-GeGaN films.

3.2. Effects of sputtering power on structural and electrical properties

Our experiments have studied the influences of RF sputtering power on structural and electrical characteristics of Zn-0.06-GeGaN films with powers at 90, 120 and 150 W. The processes were kept at 300 °C for 30 min with the Ar and N_2 flow rates of 5 sccm and 15 sccm, respectively. As shown in Table 1. The atomic ratios of [Zn]/([Zn] + [Ge] + [Ga]) were 2.6, 7.9 and 11.5 at% for Zn-0.06-GeGaN films grown at 90, 120 and 150 W, respectively, while the [Ge]/([Zn] + [Ge] + [Ga]) ratios were 3.2, 3.7, and 4.2 at% and the[N]/([Zn] + [Ge] + [Ga]) ratios were 0.937, 0.876, and 0.811. Under different output RF power condition, the Zn and Ge contents became higher and the nitrogen content lower at the higher RF power. The reason for the lower N content is due to the higher Zn content at higher RF power. As Zn^{2+} with a lower charge valency replace Ga^{3+}, the total positive charge amount decreases. To keep the charge neutrality, N^{3-} can be removed to decrease the total negative charge amount, which lead to the lower N content. An optimal growth condition is required for the reactive sputtering of Zn-*x*-GeGaN. In 2005, M. A. Reshchikov showed that there was the deficient gallium in n-type doped GaN and p-type GaN had the state of nitrogen-vacancy [34].

Fig. 1b shows the XRD patterns of Zn-0.06-GeGaN thin films. Zn-0.06-GeGaN films exhibited a wurtzite structure and polycrystalline. At 90 W of power, the grown Zn-0.06-GeGaN film had poor crystallinity because there was an insufficient momentum of the atoms migrating on the substrate during the deposition. The $(10\bar{1}0)$, $(10\bar{1}1)$ and $(11\bar{2}0)$ diffraction peaks were found with no other second phases. The diffraction peak of $(10\bar{1}0)$ located at 32.25°, 32.33°, and 32.40° for the Zn-0.06-GeGaN films deposited at RF powers of 90, 120, and 150 W, respectively. The $(10\bar{1}0)$ peak shifted to higher diffraction angle at higher RF power due to the lattice shrinkage. The lattice constant of *a, c*, and volume of a unit cell of Zn-0.06-GeGaN films in Table 2 slightly decreased with higher output power. While lattice constant of *c* slightly decreased from 5.83 Å at 90 W to 5.29 Å at 150 W, the lattice constant of *a* dropped from 3.59 to 3.25 Å and cell volume correspondingly from 64.87 to 48.43 Å^3 due to the nitrogen vacancy together with the increase of the Zn content in films. Additionally, from data shown in Table 2, the FWHM values of $(10\bar{1}0)$ peak for the deposited Zn-0.06-GeGaN films at 90, 120, and 150 W had a decrease from 0.38° to 0.28°, which further confirmed that there was better crystallinity in a thin film deposited at higher sputtering power.

SEM images in Fig. 6 exhibited the dense surface and the nanometer grains without voids and fracture. The cross-section SEM images showed the columnar growth of Zn-0.06-GeGaN films. The thicknesses of the Zn-0.06-GeGaN films sputtered at 90, 120, and 150 W in power were 0.85, 1.0 and 2.0 µm, respectively and the growth rates of 28.3, 33.3 and 66.7 nm/min. The film became thicker at higher RF power. The rms roughness values of Zn-0.06-GeGaN films deposited at 90, 120, and 150 W were 0.51, 1.61, and 2.37 nm, respectively. The faster growth rate leads to the rougher surface due to the strong argon bombardment to the target at a higher RF power, which led to a faster growth rate.

All the Zn-0.06-GeGaN films deposited at different output powers remained as *p*-type semiconductors. As shown in Fig. 4b, n_p was 4.27×10^{15}, 7.21×10^{16}, and 5.49×10^{18} cm^{-3}, µ was 150, 39.1, and 8.92 cm^2 V^{-1} s^{-1}, and σ was 0.1, 0.45, and 7.85 S cm^{-1} for Zn-0.06-GeGaN deposited at 90, 120, and 150 W, respectively. The hole concentration and electrical conductivity increased as the sputtering power rose. The higher Zn content at higher power leads to the higher conductivity.

As shown in Fig. 5b, the extrapolated E_g values were 3.17, 2.98, and 2.95 eV for Zn-0.06-GeGaN films under different RF powers of 90, 120, and 150 W, respectively. As the sputtering power increased from 90 W to 150 W, the energy band gap gradually became smaller with a decrement of 0.22 eV. It is concluded that the increased Zn content in Zn-0.06-GeGaN solid solution film results in the narrow of the energy gap due to the coexistence of the Ge_{Ga} donor level and Zn_{Ga} acceptor level.

In our system, the higher Zn content in Zn-x-GeGaN led to a larger FWHM value, smaller crystalline size, lower deposition rate, the rougher surface, higher hole concentration, and high electrical conductivity. From all this information, it refers that the Zn addition had changed the growth kinetics from the layer mode to the island mode [35]. It can related to the Zn element to favor the nucleation of small clusters and the following three-dimensional growth. These nuclei favors the cluster formation and the island growth. However, the clusters lost the adherence and could escape from the surface to lead to the lower growth rate. On the other hand, the layer mode growth had the nuclei well adherent to substrate surface, so the faster growth rate.

3.3. The hetero-junction diode devices made by Zn-x-GeGaN films

In our experiment, Zn-0-GeGaN and Zn-0.03-GeGaN films maintained *n*-type semiconductors and Zn-0.06-GeGaN and Zn-0.09-GeGaN films became *p*-type ones. The hetero-junction devices were made by the Zn-0-GeGaN and Zn-0.03-GeGaN films deposited on *p*-Si substrates to form device-A and device-B, respectively. The *p*-Zn-GeGaN/*n*-Si hetero-junction diodes were fabricated by the Zn-0.06-GeGaN and Zn-0.09-GeGaN films grown on *n*-Si substrates to form device-C and device-D, respectively. Fig. 7 shows the current density-voltage (I-V) properties

Fig. 6. (a,b,c) SEM surface images and (d,e,f) 3D AFM morphologies of Zn-0.06-GeGaN films deposited at (a,d) 90 W, (b,e) 120 W, and (c,f) 150 W in Ar/N_2 atmosphere. The insets present their single cross-sectional images.

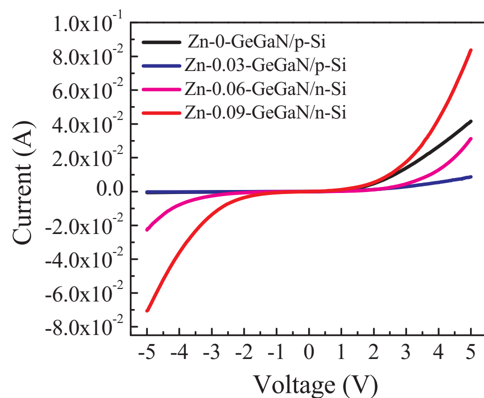

Fig. 7. The reverse and forward current-voltage (I-V) plots of Zn-*x*-GeGaN/Si layer diodes tested at room temperature.

of the device-A, -B, -C, and -D measured at room temperature from − 5–5 V. Data from the I-V curves showed that the turn-on voltages were found in 1.0, 1.0, 1.0, and 0.75 V for device-A, -B, -C, and -D, respectively. Table 4 presents the parameters and the electrical

Table 4
The parameters and the electrical characteristics of Zn-*x*-GeGaN/Si diodes.

x in Ge-*x*-GaN	Leakage current density (A/cm^2) at − 1 V	Schottky barrier height (eV)	*I-V*	Cheung's *dV/dlnI versus I*	
			n	R_S (kΩ)	n
0	-2.30×10^{-6}	0.55	5.24	0.10	5.23
0.03	-1.70×10^{-6}	0.58	4.76	0.25	4.68
0.06	-1.21×10^{-5}	0.56	4.58	0.39	4.59
0.09	-6.41×10^{-5}	0.53	3.91	0.11	3.90

characteristics of Zn-*x*-GeGaN/Si diodes. The data indicates that the reduction of turn-on voltage is related to the lower barrier height. The leakage current density at − 1 V were -2.30×10^{-6}, -1.70×10^{-6}, -1.21×10^{-5}, and -6.41×10^{-5} A cm^{-2} for Zn-*x*-GeGaN diodes at $x = 0$, 0.03, 0.06, and 0.09, respectively. At the 5 V forward bias, the highest current density was 8.37×10^{-2} A/cm^2 for the device-D. Besides, device-B had the lowest forward current densities of 8.65×10^{-3} A/cm^2, while device-A and device-C had the forward current densities of 4.16×10^{-2} and 3.13×10^{-2} A/cm^2, respectively. As displayed in the I-V plots, the breakdown voltages were > 5.0, > 5.0, 2.0, and

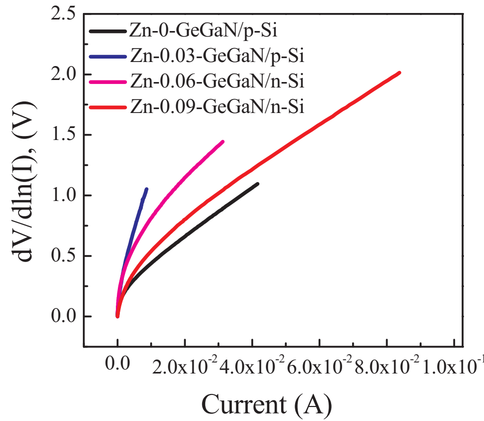

Fig. 8. Plots of dV/dln(I) versus current for Zn-*x*-GeGaN/Si diodes.

1.5 V for device-A, -B, -C and -D, respectively. The variations of leakage current density and forward current density of diodes are consistent with the electrical property in Fig. 4(a). Basically, the higher conductivity of the Zn-*x*-GeGaN film can lead to the higher leakage current, the higher forward current, the lower barrier height, and the lower turn-on voltage. The easy breakdown all occurred for device-C and device-D with the p-type Zn-*x*-GeGaN inside. The possible reason can be the higher defect density in Zn_{Ga} and Ge_{Ga} and the nature of the deep trapped energy level for Zn_{Ga}, which leads a short tunneling path at junction to breakdown.

The electrical characteristics of the diode can be calculated (for $qV > 3kT$), based on a standard thermionic-emission (TE) model. It is showed as the equation: [22,24,36,37]

$$I = I_0 \cdot \exp\left[\frac{q}{nKT}(V - IR_S)\right] \tag{2}$$

where I_0 is the saturation current, q the electron charge (1.60×10^{-19} C), V is the applied voltage, K Boltzmann constant (1.38×10^{-23} J K^{-1}), n the ideality factor, R_s the series resistance, and T the experiment temperature in Kelvin. Eq. (2) was employed to plot the curve of *ln*I versus V. The saturation current I_0 can be obtained by intersecting the interpolated straight line from the linear region of the semilog plot. The barrier height of diode can be computed by applying Eq. (3) [22,27,37].

$$\phi_B = \frac{KT}{q}\ln\left[\frac{AA^*T_2}{I_O}\right] \tag{3}$$

where A is the area of the diode with the dimension of 1×1 mm^2, A^* the effective Richardson constant and ϕ_B the barrier height. In this equation, for *n*-GaN and *p*-GaN diodes, the value in theory of A^* was computed to be 26.4 A cm^{-2} K^{-2} with $m^* = 0.22\,m_e$ while for *n*-InGaN diodes, the A^* was counted to be 23 A cm^{-2} K^{-2} with $m^* = 0.19\,m_e$ [22,27]. The ideality factor n can be achieved by the slope of the linear region in forward bias [22,27]. It can be calculated from the equation below:

$$n = \left(\frac{q}{KT}\right)\cdot\left(\frac{dV}{d(\ln I)}\right) \tag{4}$$

The dV/d(lnI) versus current figure was plotted by Eq. (4) and shown in Fig. 8. The ideality factor *n* can be calculated to be 5.24, 4.76, 4.58 and 3.91, the barrier height ϕ_B 0.55, 0.58, 0.56, and 0.53 eV for device-A, -B, -C and -D, respectively. The electrical properties of the device-A, -B, -C and -D diodes are listed in Table 4.

It is interesting that R_s and n can be obtained by Cheung's method [38,39] which is expressed as below:

$$\left(\frac{dV}{d(\ln I)}\right) = \frac{nKT}{q} + IR_S \tag{5}$$

Table 4 also showed the series resistance R_s and ideality factor n for the hetero-junction diodes. The ideality factor n was 5.23, 4.68, 4.59, and 3.90 and the series resistance R_S was 0.10, 0.25, 0.39, and 0.11 kΩ for the device-A, -B, -C, and -D, respectively.

4. Conclusions

Zn acceptor/Ge donor-codoped GaN films have been deposited on Si (100) substrates by RF reactive sputtering technology with single cermet targets. The microstructure, electrical and optical properties were investigated by SEM, AFM, TEM, XRD, UV–Vis spectrometry, and Hall measurement system. The Zn-*x*-GeGaN films at different Zn contents possessed the wurtzite structure and were polycrystalline with a preferential ($10\bar{1}0$) growth plane. The Zn-*x*-GeGaN films transformed from *n*-type Zn-x-GeGaN at $x = 0$ and 0.03 into *p*-type Zn-*x*-GeGaN semiconductor at $x = 0.06$ and 0.09. The highest conductivity was found to be 6.30 S.cm^{-1} for the Zn-0.09-GeGaN film due to its highest hole concentration of 1.38×10^{18} cm^{-3} and 28.6 cm^2 V^{-1} S^{-1} in electrical mobility. Bandgap for Zn-*x*-GeGaN films was found in the range of 2.87–3.0 eV with the Zn-0.09-GeGaN film to have the lowest one of 2.87 eV due to the coexistence of Zn_{Ga} acceptor and Ge_{Ga} donor defects. Zn-0.06-GeGaN films deposited at different sputtering powers were also investigated. All the film properties are strongly correlated to the film composition. The higher Zn content in films due to the target or RF power can have higher hole concentration and electrical conductivity, lower nitrogen content and more nitrogen vacancies, smaller cell volume, and smaller bandgap, while the surface roughness is related to the growth rate. For the *n*-Zn-*x*-GeGaN/*p*-Si diodes at $x = 0$ and 0.03 and *p*-Zn-*x*-GeGaN/*n*-Si diodes at $x = 0.06$ and 0.09, they had leakage current density of 10^{-5}~10^{-6} A/cm^2 at -1 V, ideality factor of 3.91–5.24, the Schottky barrier height of 0.53–0.58 eV, and the series resistance of 0.10–0.39 kΩ. Codoping of Zn acceptor and Ge donor in GaN has shown the significant effects on material properties and device performance.

Acknowledgments

This work was supported by the Ministry of Science and Technology of the Republic of China under grant numbers 104-2221-E-011-169-MY3, 106-2218-E-011-018, and 106-3111-Y-042A-093.

References

[1] S.C. Jain, M. Willander, J. Narayan, R.V. Overstraeten, III–nitrides: growth, characterization, and properties, J. Appl. Phys. 87 (3) (2000) 965–1006.
[2] N. Shuji, M. Takashi, S. Masayuki, High-power gan P-N junction blue-light-emitting diodes, Jpn. J. Appl. Phys. 30 (12A) (1991) L1998.
[3] N. Shuji, S. Masayuki, N. Shin-ichi, I. Naruhito, Y. Takao, M. Toshio, K. Hiroyuki, S. Yasunobu, InGaN multi-quantum-well-structure laser diodes with cleaved mirror cavity facets, Jpn. J. Appl. Phys. 35 (2B) (1996) L217.
[4] N. Shuji, M. Takashi, S. Masayuki, Si- and Ge-doped gan films grown with gan buffer layers, Jpn. J. Appl. Phys. 31 (9R) (1992) 2883.
[5] S.I. Molina, A.M. Sánchez, F.J. Pacheco, R. García, M.A. Sánchez-García, F.J. Sánchez, E. Calleja, The effect of Si doping on the defect structure of GaN/AlN/Si(111), Appl. Phys. Lett. 74 (22) (1999) 3362–3364.
[6] S. Nakamura, T. Mukai, M. Senoh, Candela-class high-brightness InGaN/AlGaN double-heterostructure blue-light-emitting diodes, Appl. Phys. Lett. 64 (13) (1994) 1687–1689.
[7] M.A. Reshchikov, M. Foussekis, J.D. McNamara, A. Behrends, A. Bakin, A. Waag, Determination of the absolute internal quantum efficiency of photoluminescence in GaN co-doped with Si and Zn, J. Appl. Phys. 111 (7) (2012) 073106.
[8] C. Chin-An, T. Tzu-Yu, C. Pen-Hsiu, C. Nie-Chuan, L. Chi-Te, Magnesium doping of In-rich InGaN, Jpn. J. Appl. Phys. 46 (5R) (2007) 2840.
[9] D.-H. Kuo, C.-C. Li, T.T.A. Tuan, W.-C. Yen, Effects of Mg doping on the performance of InGaN films made by reactive sputtering, J. Electron. Mater. 44 (1) (2015) 210–216.
[10] T.T.A. Tuan, D.-H. Kuo, A.D. Saragih, G.-Z. Li, Electrical properties of RF-sputtered Zn-doped GaN films and p-Zn-GaN/n-Si hetero junction diode with low leakage current of 10 − 9A and a high rectification ratio above 105, Mater. Sci. Eng.: B 222 (Supplement C) (2017) 18–25.
[11] K. Yohannes, D.-H. Kuo, Growth of p-type Cu-doped GaN films with magnetron sputtering at and below 400 °C, Mater. Sci. Semicond. Process. 29 (Suppl. C) (2015)

288–293.
[12] C. Freysoldt, B. Grabowski, T. Hickel, J. Neugebauer, G. Kresse, A. Janotti, C.G. Van de Walle, First-principles calculations for point defects in solids, Rev. Mod. Phys. 86 (1) (2014) 253–305.
[13] S.-H. Wei, Overcoming the doping bottleneck in semiconductors, Comput. Mater. Sci. 30 (3) (2004) 337–348.
[14] J. Zhang, K. Tse, M. Wong, Y. Zhang, J. Zhu, A brief review of co-doping, Front. Phys. 11 (6) (2016) 117405.
[15] H. Katayama-Yoshida, T. Nishimatsu, T. Yamamoto, N. Orita, Codoping method for the fabrication of low-resistivity wide band-gap semiconductors in p-type GaN, p-type AlN and n-type diamond: prediction versus experiment, J. Phys.: Condens. Matter 13 (40) (2001) 8901.
[16] H. Katayama-Yoshida, R. Kato, T. Yamamoto, New valence control and spin control method in GaN and AlN by codoping and transition atom doping, J. Cryst. Growth 231 (3) (2001) 428–436.
[17] K.S. Kim, G.M. Yang, H.J. Lee, The study on the growth and properties of Mg doped and Mg–Si codoped p-type GaN, Solid-State Electron. 43 (9) (1999) 1807–1812.
[18] K.S. Kim, M.S. Han, G.M. Yang, C.J. Youn, H.J. Lee, H.K. Cho, J.Y. Lee, Codoping characteristics of Zn with Mg in GaN, Appl. Phys. Lett. 77 (8) (2000) 1123–1125.
[19] S. Nakamura, G. Fasol, The Blue Laser Diode: GaN Based Light Emitters and Lasers, Springer, Berlin; New York, 1997.
[20] J.K. Sheu, C.J. Pan, G.C. Chi, C.H. Kuo, L.W. Wu, C.H. Chen, S.J. Chang, Y.K. Su, White-light emission from InGaN-GaN multiquantum-well light-emitting diodes with Si and Zn codoped active well layer, IEEE Photonics Technol. Lett. 14 (4) (2002) 450–452.
[21] C.-C. Li, D.-H. Kuo, Material and technology developments of the totally sputtering-made p/n GaN diodes for cost-effective power electronics, J. Mater. Sci.: Mater. Electron. 25 (4) (2014) 1942–1948.
[22] T.T.A. Tuan, D.-H. Kuo, C.-C. Li, W.-C. Yen, Schottky barrier characteristics of Pt contacts to all sputtering-made n-type GaN and MOS diodes, J. Mater. Sci.: Mater. Electron. 25 (8) (2014) 3264–3270.
[23] D.-H. Kuo, T.T.A. Tuan, C.-C. Li, W.-C. Yen, Electrical and structural properties of Mg-doped InxGa1–xN (x ≤ 0.1) and p-InGaN/n-GaN junction diode made all by RF reactive sputtering, Mater. Sci. Eng.: B 193 (2015) 13–19.
[24] C.-C. Li, D.-H. Kuo, P.-W. Hsieh, Y.-S. Huang, Thick In x Ga1–x N films prepared by reactive sputtering with single cermet targets, J. Electron. Mater. 42 (8) (2013) 2445–2449.
[25] C.-W. Ting, C.P. Thao, D.H. Kuo, Electrical and structural characteristics of tin-doped GaN thin films and its hetero-junction diode made all by RF reactive sputtering, Mater. Sci. Semicond. Process. 59 (2017) 50–55.
[26] C.-C. Li, D.-H. Kuo, Effects of growth temperature on electrical and structural properties of sputtered GaN films with a cermet target, J. Mater. Sci.: Mater. Electron. 25 (3) (2014) 1404–1409.
[27] T.T. Anh Tuan, D.-H. Kuo, Characteristics of RF reactive sputter-deposited Pt/SiO2/n-InGaN MOS Schottky diodes, Mater. Sci. Semicond. Process. 30 (2015) 314–320.
[28] H.W. Kim, N.H. Kim, Preparation of GaN films on ZnO buffer layers by rf magnetron sputtering, Appl. Surf. Sci. 236 (1–4) (2004) 192–197.
[29] I. Chyr, B. Lee, L.C. Chao, A.J. Steckl, Damage generation and removal in the Ga+ focused ion beam micromachining of GaN for photonic applications, J. Vac. Sci. Technol. B 17 (6) (1999) 3063–3067.
[30] C.P. Thao, D.H. Kuo, Electrical and structural characteristics of Ge-doped GaN thin films and its hetero-junction diode made all by RF reactive sputtering, Mater. Sci. Semicond. Process. 74 (Supplement C) (2018) 336–341.
[31] J. Neugebauer, C.G. Van de Walle, Atomic geometry and electronic structure of native defects in GaN, Phys. Rev. B 50 (11) (1994) 8067–8070.
[32] A. Shikanaia, H. Fukahori, Y. Kawakami, K. Hazu, T. Sota, T. Mitani, T. Mukai, S. Fujita, Optical properties of Si-, Ge- and Sn-doped GaN, Phys. Status Solidi (b) 235 (1) (2003) 26–30.
[33] T. Mattila, R.M. Nieminen, Point-defect complexes and broadband luminescence in GaN and AlN, Phys. Rev. B 55 (15) (1997) 9571–9576.
[34] M.A. Reshchikov, H. Morkoç, Luminescence properties of defects in GaN, J. Appl. Phys. 97 (6) (2005) 061301.
[35] M. Ohring, Chapter 5 – Plasma and Ion Beam Processing of Thin Films, Materials Science of Thin Films, Second edition, Academic Press, 2002, pp. 203–275.
[36] R.K. Gupta, F. Yakuphanoglu, K. Ghosh, P.K. Kahol, Fabrication and characterization of p–n junctions based on ZnO and CuPc, Microelectron. Eng. 88 (10) (2011) 3067–3069.
[37] R. Padma, B. Prasanna Lakshmi, M. Siva Pratap Reddy, V. Rajagopal Reddy, Electrical and structural properties of Ir/Ru Schottky rectifiers on n-type InGaN at different annealing temperatures, Superlattices Microstruct. 56 (2013) 64–76.
[38] S. Bengi, M.M. Bülbül, Electrical and dielectric properties of Al/HfO2/p-Si MOS device at high temperatures, Curr. Appl. Phys. 13 (8) (2013) 1819–1825.
[39] S.K. Cheung, N.W. Cheung, Extraction of Schottky diode parameters from forward current-voltage characteristics, Appl. Phys. Lett. 49 (2) (1986) 85–87.